Quaternary Geochronology 39 (2017) 174–188

Contents lists available at ScienceDirect

Quaternary Geochronology

journal homepage: www.elsevier.com/locate/quageo

Research paper

Radiocarbon-calibrated amino acid racemization ages from Holocene sand dollars (*Peronella peronii*)

Matthew A. Kosnik [a, *], Quan Hua [b], Darrell S. Kaufman [c], Michał Kowalewski [d], Katherine Whitacre [c]

[a] Department of Biological Sciences, Macquarie University, New South Wales 2109, Australia
[b] Australian Nuclear Science and Technology Organisation, Locked Bag 2001, Kirrawee DC, New South Wales 2232, Australia
[c] School of Earth Sciences & Environmental Sustainability, Northern Arizona University, Flagstaff, AZ 86011-4099, USA
[d] Florida Museum of Natural History, University of Florida, Gainesville, FL 32611, USA

ARTICLE INFO

Article history:
Received 25 September 2016
Received in revised form
23 October 2016
Accepted 5 December 2016
Available online 24 December 2016

ABSTRACT

Amino acid racemization (AAR) is widely used as a cost-effective method to date molluscs in time-averaging and taphonomic studies, but it has not been attempted for echinoderms despite their paleobiological importance and distinct biomineralization. Here we demonstrate the applicability of AAR geochronology for dating Holocene *Peronella peronii* (Echinodermata: Echinoidea) collected from Sydney Harbour (Australia). Using standard HPLC methods we determined the extent of AAR in 74 *Peronella* tests and performed replicate analyses on 23 tests. Replicate analyses from the outer edge of 23 tests spanning the observed range of D/L values yielded median coefficients of variation <4% for Asp, Glu, and Phe D/L values, which is comparable to the analytical precision. Correlations between THAA D/L values across 178 independently prepared subsamples of 74 individuals are also very high (Spearman $\rho \geq 0.95$) for these three amino acids. The ages of 20 individuals spanning the observed range of D/L values were determined using ^{14}C analyses, and Bayesian model averaging was used to determine the best AAR age model. Only three models fit to Glu D/L contributed to the final averaged age model. Modeled ages ranged from 14 to 5496 years, and the median 95% confidence interval for the 54 AAR ages was ±29% of the modelled age. In comparison, the median 2σ confidence interval for nine graphite target ^{14}C ages was ±8% of the median age estimate and the median 2σ confidence interval for 20 carbonate target ^{14}C ages was ±26% of the median age estimate. Overall *Peronella* yield high-quality D/L values and appear to be a good target for AAR geochronology.

1. Introduction

Calibrated amino acid racemization (AAR) ages are widely used to date fossils found in Holocene deposits. The unique qualities of AAR have been key to determining the extent of time-averaging in molluscan material from a wide variety of locations, notably the central and southern Great Barrier Reef, Australia (Kosnik et al., 2007, 2009, 2013, 2015), Sydney Harbour, Australia (Dominguez et al., 2016), the Gulf of California, Mexico (Kowalewski et al., 2000), Texas (Olszewski and Kaufman, 2015), Panama (Kidwell et al., 2005), and Brazil (Krause et al., 2010; Dexter et al., 2014). Although these research projects have been transforming our understanding of how fossil deposits form and the timescales they record, the focus has been largely on bivalves from the order Veneroida collected from shallow-water marine environments. Aside from bivalves, time-averaging has been quantified only in a few case studies, including marine gastropods from the central Great Barrier Reef (Kosnik et al., 2009, 2013), terrestrial gastropods from the Canary Islands (Yanes et al., 2007), and brachiopods from the Brazilian shelf (Carroll et al., 2003; Barbour Wood et al., 2006; Krause et al., 2010). While the last decade has seen tremendous activity, the patterns and processes of time-averaging will only be fully revealed through studies on additional taxa encompassing a broader range of taphonomic durability and depositional settings.

Echinoids are an important part of marine ecosystems (Kroh and Smith, 2010), and their mineralised skeletal elements make them

* Corresponding author.
E-mail addresses: mkosnik@alumni.uchicago.edu (M.A. Kosnik), qhx@ansto.gov.au (Q. Hua), Darrell.Kaufman@nau.edu (D.S. Kaufman), kowalewski@ufl.edu (M. Kowalewski), Katherine.Whitacre@nau.edu (K. Whitacre).

http://dx.doi.org/10.1016/j.quageo.2016.12.001
1871-1014/

important contributors to biogenic sediment and the fossil record (Nebelsick and Kroh, 2002 and references therein). Echinoid skeletons, termed "tests", are composed of calcite plates, so they are typically prone to fragmentation (Allison, 1990; Greenstein, 1991, 1992, 1993; Nelbelsick, 2004). Sand dollars are extremely flattened clypeasteroid echinoids with particularly robust tests, relative to other echinoids, due to interlocking plates and internal supports (Seilacher, 1979; Nebelsick, 1999). Although echinoderms are a key component of marine soft-sediment ecosystems and the fossil record, they have not been evaluated as potential candidates for AAR.

While AAR has been applied to a wide variety of sample types, the accuracy of the method requires biominerals that effectively retain the constituent amino acids of their original proteins (Miller et al., 2013). Thus, the efficacy of AAR must be evaluated on a taxon-by-taxon basis. Determining a taxon's suitability for AAR entails quantifying 1) amino acid variation within a specimen, 2) precision/repeatability of D/L measurements, and 3) the strength of the relation between D/L and the numerical age of the specimen estimated independently (most commonly via AMS radiocarbon dating). Ideally, a taxon has low within-skeleton variation, but minimally a suitable area for sampling must be determined. Replicate samples of the same material must yield the same D/L values, at least for a useful subset of possible amino acids. The ultimate precision of any modelled ages will be limited by the strength of the modelled relation between D/L and independently determined ages. Here we evaluate each of these criteria using Holocene *Peronella peronii* tests collected from Sydney Harbour.

2. Sample description

Sand dollars were collected from sub-aqueous Holocene sediments in Sydney Harbour, New South Wales, Australia (Watsons Bay [33.84233°S, 151.27757°E, 10.4 m water depth] and Little Manly Cove [33.80897°S, 151.28543°E, 7.9 m water depth]) using diver-operated dredges as part of ongoing investigations into the harbor's historical and present-day benthic communities. The Watsons Bay material was collected from various layers of a 1.8-m-deep excavation, whereas the Little Manly Cove material was sampled from the surficial 0.2 m (see: Dominguez et al., 2016, for additional information on the sampling localities). Complete *Peronella peronii* (Agassiz, 1841) (Echinodermata, Echinoidea, Clypeasteroida, Laganidae) (Fig. 1) tests are relatively common in sandy Sydney Harbour sediments, although despite extensive sampling no live individual was found during our sampling or recently by other collectors (e.g., Miskelly, 2002). This species, a deposit feeder preferentially inhabiting fine sand substrates (Miskelly, 2002), is endemic to Australia. It is widely distributed in temperate Australian waters. Like most sand dollars, it possesses a test that is more robust than most echinoderms, while being considerably more fragile than most molluscan shells.

While sand dollars are considerably rarer than molluscan shells, we were able to sample 74 essentially intact specimens encompassing a broad range of ages for this study from two sites. The 16 *Peronella* collected from Little Manly surface samples were all expected to be post-colonial (since 1788 AD) in age, whereas the 58 *Peronella* collected opportunistically from six layers (2 specimens from 0.84 to 0.88 m, 8 from 0.98 to 1.03 m, 17 from 1.13 to 1.18 m, 11 from 1.28 to 1.33 m, 15 from 1.43 to 1.48 m, and 5 from 1.58 to 1.63 m) of the Watsons Bay excavation were expected to span the last ~ 6 ka (Dominguez et al., 2016).

Sand dollars are extremely flattened and pentaradially symmetric (Fig. 1). Initially two *Peronella* tests, one old and one young (based on their initial AAR estimates), were sampled three times in four areas to evaluate within-test variability and the variation among replicate samples. The four areas sampled were the: aboral side (Fig. 1A), oral side (Fig. 1B), teeth/lantern (four teeth are visible in Fig. 1B), and outer edge. The outer edge tends to be the most robust portion of the test, and it is preserved even in the most broken specimens. The oral and aboral sides represent the largest area of the test even though they are most often damaged. The teeth have the potential to be found in isolation of the remainder of the test in smaller sieve size fractions, and they are mineralogically and structurally distinct (Ma et al., 2009; Killian et al., 2009; Yang et al., 2011). An additional 72 tests were sampled only from the outer edge of the test. The median geometric mean size of the dated tests was 12 mm (6–19 mm) and the median mass was 705 mg (99–3007 mg). Comprehensive specimen information is provided in Appendix A.

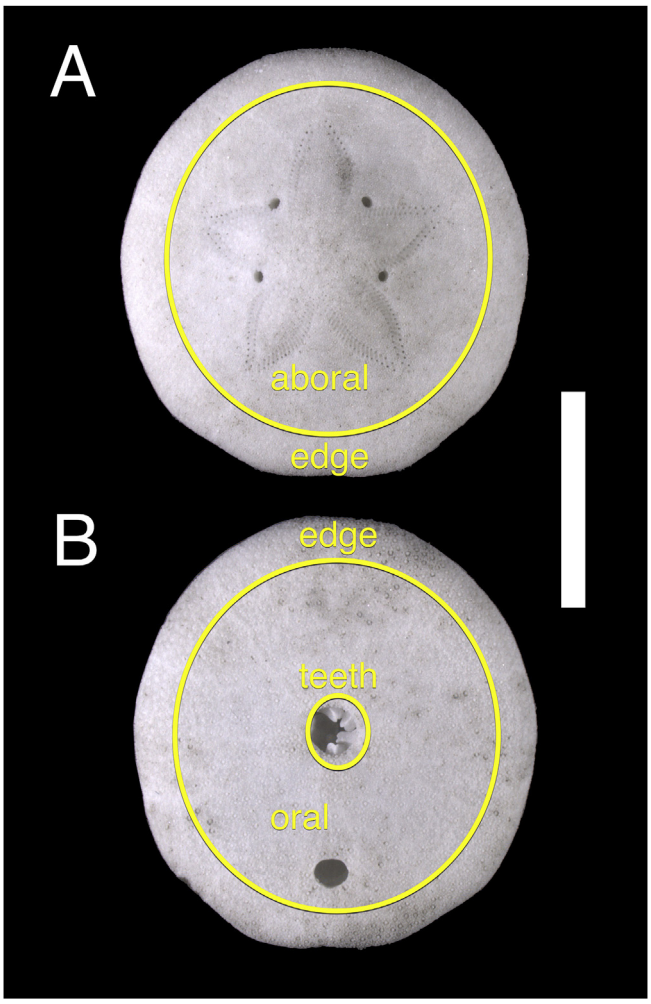

Fig. 1. A *Peronella peronii* test collected from Sydney Harbour. (A) The aboral side. (B) The oral side, and four teeth are visible through the oral hole. The scale bar is 10 mm. The photographed specimen is deposited in the Paleontology collection at the Australian Museum, Sydney (F.142367).

3. Methods

3.1. Amino acid racemization

Samples from 74 tests were prepared for amino acid analysis according to standard procedure (Wehmiller and Miller, 2000). The

tests were broken to subsample fragments from specific anatomical positions (Fig. 1). Selected fragments, ranging from 10 to 50 mg, were cleaned by acid leaching to remove 30% of the mass, then demineralized in 20 μl of 7 M HCl per mg of $CaCO_3$. The total hydrolysable amino acid (THAA) population was recovered by hydrolysing the sample solutions under N_2 at 110 °C for 22 h, whereas free amino acid (FAA) samples were dried in-vacuo immediately after adding acid, then rehydrated and analyzed without additional heating.

To examine differences between intra- vs. extra-crystalline amino acid populations, fragments from 23 tests were also prepared with an additional bleaching step to eliminate all but intra-crystalline amino acids (Penkman et al., 2008; Demarchi et al., 2013). Tests were ground and sieved to obtain test fragments between 90 and 425 μm. These fragments were placed into 12% NaOCl (sodium hypochlorite) at a ratio of 50 μl per mg of sample. The bleach-suspended samples were vortexed, then left in bleach for 48 h, vortexing again after 24 h. After 48 h they were rinsed five times with reagent grade H_2O, then rinsed once with methanol and allowed to dry. The resulting samples were analysed for THAA and FAA.

Sample solutions were evaporated to dryness in vacuo, then rehydrated in 0.01 M HCl containing an internal standard of L-*homo*-arginine (L-*h*Arg) of known concentration for calculating the concentration of amino acids relative to the mass of test. Each sample solution was analyzed once using reverse-phase, high-performance liquid chromatography (HPLC). All chromatograms were of consistently high quality (e.g., Fig. 2) and none was rejected. The chromatographic instrumentation and procedure used to separate amino acid enantiomers is detailed in Kaufman and Manley (1998). The analytical method employed pre-column derivatization with *o*-phthaldialdehyde together with the chiral thiol, N-isobutyryl-L-cysteine, to yield fluorescent diastereomeric derivatives of chiral (D and L) amino acids. The derivatization was performed on-line prior to each injection using the auto-injector of an integrated Agilent 1100 HPLC. Separation was by a reverse-phase column packed with a C_{18} stationary phase (HyperClone™ BDS, 5 μm, 250 × 3.2 mm) using a linear gradient of aqueous sodium acetate, methanol and acetonitrile. Detection was by fluorescence.

For this study we focused on the eight amino acids that are typically abundant and resolvable by reverse-phase HPLC: aspartic acid (Asp), glutamic acid (Glu), serine (Ser), alanine (Ala), valine (Val), phenylalanine (Phe), isoleucine (Ile), and leucine (Leu). The Asp and Glu concentration values may be slightly overestimated because minor amounts of asparagine and glutamine may convert during laboratory hydrolysis to Asp and Glu, respectively. AAR data for all eight amino acids are reported in Appendix A.

3.2. Radiocarbon dating

As discussed above, *Peronella* is a deposit feeder consuming detritus from the sea floor. In areas dominated by limestone geologies or sediment containing large amounts of reworked carbonate, this older carbon can be incorporated into the animal skeleton biasing radiocarbon analyses (Petchey, 2009; Hua, 2015). However, the Sydney basin is carbonate poor and the sediment in Sydney Harbour is dominantly siliciclastic, suggesting that the carbon used by *Peronella* in Sydney Harbour to build their tests is likely to be isotopically marine. Thus Sydney Harbour *Peronella* should be well suited to radiocarbon dating.

Twenty individuals spanning the range of observed D/L values

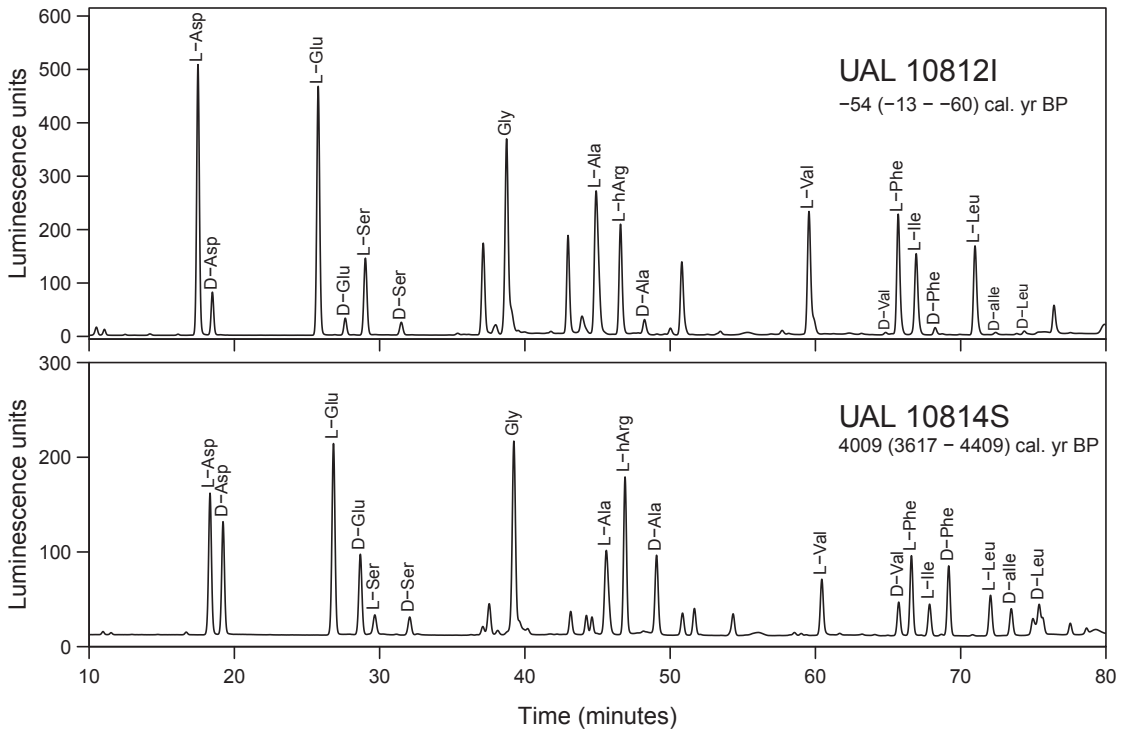

Fig. 2. Two representative chromatograms from *Peronella* (unbleached THAA). Y-axis in luminescence units and x-axis in minutes after injection. UAL-10812I and UAL-10814S illustrate low levels of background. Age of specimen in calibrated radiocarbon ages before 1950 (cal. year BP) with 95% confidence interval. Amino acid peaks are labelled including L-*h*Arg, which is used as an internal standard. As seen in UAL-10814S, the D-Leu peak occasionally has a co-eluting compound. In these cases, the smaller co-eluting peak to the left was split from the D-Leu peak.

were selected for ^{14}C dating using the suite of criteria outlined in Kosnik et al. (2008) and the analyses are presented in Sections 4.2–4.4 below. Prior to submission for radiocarbon analysis, test fragments were sonicated and rinsed in reagent-grade H_2O and ~30% of the remaining mass was removed with 2 M HCl. All 20 individuals (two in duplicate, sampled and analyzed at different times) were analysed using powdered carbonate targets, which simplifies the procedure but reduces the precision (Bush et al., 2013). Three tests were analysed by Accelerator Mass Spectrometry (AMS) following conversion to graphite targets at the Australian Nuclear Science and Technology Organisation (ANSTO) using the STAR facility (Fink et al., 2004). Six individuals were analysed by AMS at University of California Irvine (UCI) following conversion to graphite targets (standard procedure). The carbonate target ^{14}C ages may be well suited for AAR calibrations of Holocene materials, as four times the number of specimens can be analyzed for the same cost, thereby increasing the number of data points used to determine of the rate of AAR (D/L versus ^{14}C age). Ages measured from graphite and carbonate targets are compared in detail in the results (Section 4.1).

Radiocarbon ages were converted to calendar years using OxCal 4.2 (Bronk Ramsey, 2009), Marine13 data (Reimer et al., 2013), and a constant regional marine reservoir correction (ΔR) value of 6 ± 50 years for the period < 5.4 cal ka BP (Dominguez et al., 2016). The median of the age probability function was used as the calendar age, and the 2σ age range was used as the age uncertainty. For the test younger than 1950 AD, the fraction of modern carbon ($F^{14}C$) was used instead of conventional ^{14}C age. These values were converted to calendar ages using a regional calibration curve for marine samples for the period from 1950 AD onward and the calibration software OxCal v4.2. The regional marine curve for the period 1950–2010 was constructed from recent coral ^{14}C data from Abraham Reef, Heron Reef and Lady Musgrave Reef (22–24°S, 152–153°E; Druffel and Griffin, 1995, 1999) and Holmes Reef (17°S, 148°E; Dawson et al., 2014) in the GBR. All amino acid ages discussed herein are calendar years relative to 2013 AD, the primary year of sample collection (2013 AD = 0 a). The results are the same with reference to any year zero (i.e., 1950 AD), but the AAR calibration models fit here are only defined for positive ages (Allen et al., 2013).

3.3. Age determination

AAR calibration curves were created using an updated version of the scripts published by Allen et al. (2013, [2016-July-17]). We used R 3.3.1 (R Development Core Team, 2016) and JAGS 4.2.0 (Plummer, 2003) to fit simple power-law kinetics (SPK), constrained power-law kinetics (CPK), and time-dependent kinetics (TDK) functions using gamma and lognormal uncertainty distributions to the three amino acid D/Ls with low coefficients of variation (see: Section 4.3 and 4.4). Scripts and outputs are included as Appendix B, including: (1) best fit model parameters for all fit models; (2) model fit graphs; (3) detailed model fits; (4) Bayesian posterior probabilities for each parameter of each model; (5) inferred ages summary; and (6) R scripts used for all analyses and to generate all plots.

4. Results and discussion

4.1. Radiocarbon dating

Two methods of AMS radiocarbon dating were used, and nine individuals were analysed using both carbonate and graphite targets. While the relation between the graphite and carbonate target ages was indistinguishable from one (Fig. 3), the carbonate target ages are systematically younger than the graphite target ages

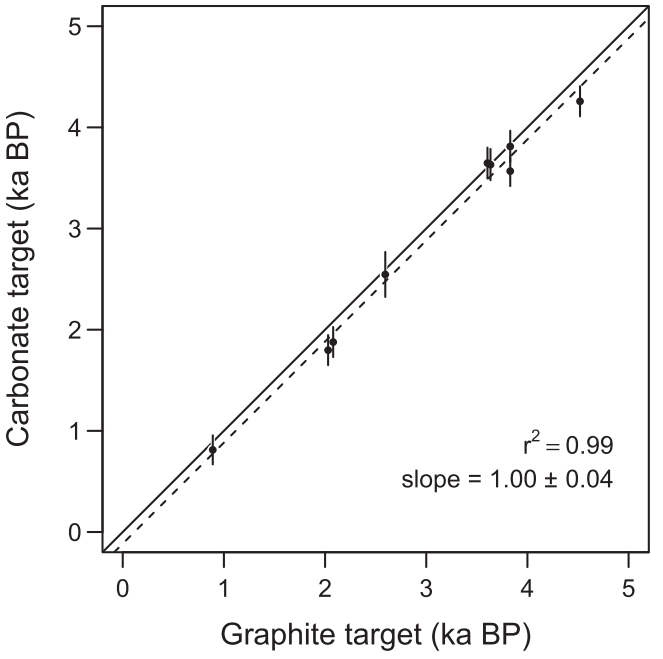

Fig. 3. Relation between ^{14}C ages on paired analyses of graphite and carbonate targets. The x-axis and y-axis are ^{14}C ka BP (thousands of uncalibrated years before 1950), the solid line represents 1:1, the dashed line represents the best fit relation, the points are conventional carbon age and 1σ error bars (x-axis uncertainties are smaller than the size of the plot symbols). Data in Table 1A.

(168 ± 126 ^{14}C years, Table 1A). This age offset may be due to an inappropriate blank material used for the AMS carbonate target analysis (Southon, pers. comm.). Blank material used was from an old speleothem free of ^{14}C (Bush et al., 2013). Less absorption of modern CO_2 by the dense calcite stalagmite blank compared to that of the more porous calcite *Peronella* test likely results in lower blank values measured in the stalagmite blank than for the *Peronella*. This leads to an underestimate of the blank correction for biogenic carbonates and consequently younger ^{14}C ages for the *Peronella* carbonate targets.

In addition to the systematic offset between graphite and carbonate targets, two specimens were analysed twice by AMS using carbonate targets. These replicate samples were independently prepared and analysed in different batches (Table 1A, specimens 20770 and 20744). While the replicate ages were generally consistent, they did not overlap within the 1σ conventional age error estimates provided (Table 1A). On the other hand, the averaged replicate carbonate target ages for the specimens did overlap the graphite target ages for the specimens. This suggests that the true uncertainty on the carbonate target ages is larger than suggested by the 1σ conventional age error reported.

The weighted mean offset between carbonate and graphite target conventional ages (168 ± 126 ^{14}C years) was determined using the nine specimens dated with both methods (Bevington and Robinson, 1992; Table 1A). To compensate for the systematic offset between carbonate and graphite target analyses, the offset was added to the conventional age estimates derived from carbonate targets, and the resulting adjusted conventional age was calibrated using the methods described in Section 3.2 (Table 1B). Applying the offset to the conventional age prior to calibration associates the correction directly with the measurement rather than after the measurement has been transformed into calendar years. The median 2σ confidence interval for the

Table 1A
Radiocarbon analyses from nine individual tests used to determine the offset between carbonate and graphite AMS targets. All ages in ^{14}C years BP and 1σ uncertainty.

Specimen	Lab	ID[a]	Target	$\delta^{13}C$	Conventional age		Difference	
					Age	1σ unc.	Age	1σ unc.
18185	UCI	137735	Graphite		890	20		
18185	UCI		Carbonate		780	70		
							110	73
18186	ANSTO	OZT206	Graphite	2.2	2030	25		
18186	UCI		Carbonate		1760	80		
							270	84
18193	UCI	163845	Graphite		3830	15		
18193	UCI		Carbonate		3530	80		
							300	81
18195	UCI	137736	Graphite		3830	20		
18195	UCI		Carbonate		3770	90		
							60	92
18275	UCI	163846	Graphite		2080	15		
18275	UCI		Carbonate		1840	80		
							240	81
20744	ANSTO	OZT207	Graphite	−3.9	3605	25		
20744	UCI		Carbonate		3510	80		
20744	UCI		Carbonate		3695	55		
20744	Weighted mean ^{14}C age of carbonate targets				3636	86		
							−31	90
20759	UCI	163844	Graphite		4520	15		
20759	UCI		Carbonate		4220	80		
							300	81
20770	UCI	163847	Graphite		2595	15		
20770	UCI		Carbonate		2300	90		
20770	UCI		Carbonate		2680	70		
20770	Weighted mean ^{14}C age of carbonate targets				2537	184		
							58	185
20771	ANSTO	OZT208	Graphite	1.2	3635	25		
20771	UCI		Carbonate		3590	90		
							45	93
Weighted mean ^{14}C age difference							**168**	**126**

[a] UCI does not issue laboratory identification numbers for carbonate target analyses.

nine *Peronella* tests with calibrated ages derived from graphite targets was ±8% of the median age estimate whereas the median 2σ interval for the 20 *Peronella* tests with calibrated ages derived from corrected carbonate targets was ±26% of the median age estimate (Table 1B).

4.2. Amino acid composition of Peronella

Amino acids extracted from *Peronella* tests using standard procedures typically yielded excellent chromatograms, with well-resolved, symmetrical peaks, consistent retention times, and stable baselines (Fig. 2). Several D-amino acids which were eluted in the latter part of the analysis, however, had small peak areas, which increased D/L variability for these amino acids (particularly Val, Phe, Ile, and Leu). Chromatograms of bleached samples were similarly well resolved.

4.2.1. Total hydrosoluble amino acid composition

To evaluate the variability and trends in the amino acid data from *Peronella*, we compared our results with available datasets from two molluscs, Holocene *Scissulina* (Mollusca: Bivalvia) and *Liloa* (Mollusca: Gastropoda) (data from Kosnik et al., 2013). The concentration of total hydrolysable amino acids (THAA) in *Peronella* tests was similar to the concentrations in *Scissulina* and *Liloa* (Fig. 4). The concentration of amino acids generally, but not universally, declined with increasing D/L in all three taxa (Fig. 4A–C). The relative abundance of amino acids showed taxon-specific differences, but in all three taxa Asp, Glu, and Ala were the most abundant (Fig. 4D–F). In *Peronella*, Asp, Ser, Val, Leu, and Ile were relatively more abundant in younger tests, whereas Glu, Ala and Phe were relatively more abundant in older tests (Fig. 4D). Demarchi et al. (2013) reported similar THAA abundance patterns in *Patella vulgata*, with Asp, Glu and Ala being the most abundant and geochronologically useful amino acids, although Asp is less abundant in these taxa than reported from *P. vulgata*. Change in the relative concentration can be an indication of closed-system behaviour or remnant protein structure (Penkman et al., 2008; Demarchi et al., 2013; Ortiz et al., 2015). The relatively narrow confidence intervals on the relative amino acid abundance plot indicate consistency across the amino acids. Ser, which has the greatest variation in relative abundance (Fig. 4D–F), is not a chronologically useful amino acid (Miller and Brigham-Grette, 1989).

4.2.2. Intra-crystalline amino acid composition

Bleaching reduced the amino acid concentration, as expected. In *Peronella*, the average intra-crystalline THAA concentration was 69% of the unbleached THAA concentration, although the decrease was less for the three most abundant amino acids (74% for Asp, Glu, Ala). The proportion of intra-crystalline amino acids is much higher than reported for *P. vulgata* in which the bleached THAA concentration is only 7–14% of the THAA unbleached concentration (Demarchi et al., 2013). The average intra-crystalline FAA concentration was 43% of the unbleached THAA concentration, although the decrease was especially pronounced in Glu (22% of unbleached THAA concentration).

The relative concentration of geochronologically important amino acids in the intra-crystalline THAA fraction was very similar to the unbleached THAA fraction, especially for the best resolved and most abundant amino acids (Asp, Glu, Ala and Phe in Fig. 5). Intra-crystalline FAA composition was distinctly different from the

Table 1B
Radiocarbon data. Specimen number and collection date, Original, weighted means, and corrected radiocarbon data. Conventional radiocarbon age (^{14}C yr), calibrated age (yr before 1950AD), and age relative to collection date used in AAR calibration analyses (yr before 2013). Calibration curve and ΔR.

Specimen		Radiocarbon metadata			Modern carbon		Age (^{14}C yr)		Age (cal yr before 2013)		ΔR	Curve
Number	Collection date	Target	Lab	Lab ID	Percent	1σ	Age	1σ	Age	2σ age range		
18185	2013-05-22	Graphite	UCI	137735	89.52	0.20	890	20	564	481–676	6 ± 50	marine13
		Carbonate	UCI		90.77	0.71	780	70	466	319–604	6 ± 50	marine13
		Carbonate	corrected				948	144	606	332–881	6 ± 50	marine13
18186	2013-05-22	Graphite	ANSTO	OZT206	77.65	0.23	2030	25	1655	1493–1801	6 ± 50	marine13
		Carbonate	UCI		80.28	0.72	1760	80	1373	1178–1584	6 ± 50	marine13
		Carbonate	corrected				1928	149	1554	1239–1917	6 ± 50	marine13
18191	2013-05-22	Carbonate	UCI		70.99	0.36	2755	45	2544	2383–2742	6 ± 50	marine13
		Carbonate	corrected				2923	134	2730	2379–3085	6 ± 50	marine13
18193	2013-05-22	Graphite	UCI	163845	62.06	0.10	3830	15	3835	3686–3983	6 ± 50	marine13
		Carbonate	UCI		64.48	0.63	3530	80	3475	3230–3703	6 ± 50	marine13
		Carbonate	corrected				3698	149	3685	3303–4108	6 ± 50	marine13
18195	2013-05-22	Graphite	UCI	137736	62.09	0.15	3830	20	3835	3680–3987	6 ± 50	marine13
		Carbonate	UCI		62.51	0.67	3770	90	3766	3503–4033	6 ± 50	marine13
		Carbonate	corrected				3938	155	3993	3587–4451	6 ± 50	marine13
18203	2013-05-22	Carbonate	UCI		62.48	0.46	3780	60	3777	3568–3984	6 ± 50	marine13
		Carbonate	corrected				3948	140	4005	3625–4423	6 ± 50	marine13
18207	2013-05-22	Carbonate	UCI		66.71	0.68	3259	90	3127	2870–3393	6 ± 50	marine13
		Carbonate	corrected				3427	155	3343	2924–3743	6 ± 50	marine13
18274	2013-05-22	Carbonate	UCI		75.45	0.44	2265	50	1929	1752–2113	6 ± 50	marine13
		Carbonate	corrected				2433	136	2138	1770–2496	6 ± 50	marine13
18275	2013-05-22	Graphite	UCI	163846	77.20	0.11	2080	15	1711	1587–1853	6 ± 50	marine13
		Carbonate	UCI		79.53	0.76	1840	80	1453	1273–1665	6 ± 50	marine13
		Carbonate	corrected				2008	149	1640	1321–1999	6 ± 50	marine13
20743	2013-05-22	Carbonate	UCI		63.84	0.89	3610	120	3573	3252–3905	6 ± 50	marine13
		Carbonate	corrected				3778	174	3789	3338–4291	6 ± 50	marine13
20744	2013-05-22	Graphite	ANSTO	OZT207	63.85	0.17	3605	25	3558	3422–3695	6 ± 50	marine13
		Carbonate	UCI		63.14	0.39	3695	55	3668	3487–3878	6 ± 50	marine13
		Carbonate	UCI		64.64	0.61	3510	80	3451	3213–3684	6 ± 50	marine13
		Carbonate	weighted mean				3636	86	3600	3382–3875	6 ± 50	marine13
		Carbonate	corrected mean				3804	153	3818	3421–4250	6 ± 50	marine13
20751	2013-05-22	Carbonate	UCI		62.51	0.36	3775	50	3770	3582–3959	6 ± 50	marine13
		Carbonate	corrected				3943	136	3997	3626–4407	6 ± 50	marine13
20757	2013-05-22	Carbonate	UCI		62.09	0.45	3830	60	3837	3626–4045	6 ± 50	marine13
		Carbonate	corrected				3998	140	4072	3680–4472	6 ± 50	marine13
20759	2013-05-22	Graphite	UCI	163844	56.98	0.08	4520	15	4774	4616–4894	6 ± 50	marine13
		Carbonate	UCI		59.12	0.57	4220	80	4366	4092–4630	6 ± 50	marine13
		Carbonate	corrected				4388	149	4599	4155–4995	6 ± 50	marine13
20769	2013-05-22	Carbonate	UCI		71.83	0.45	2660	60	2418	2198–2676	6 ± 50	marine13
		Carbonate	corrected				2828	140	2617	2241–2967	6 ± 50	marine13
20770	2013-05-22	Graphite	UCI	163847	72.37	0.10	2595	15	2322	2176–2449	6 ± 50	marine13
		Carbonate	UCI		71.62	0.54	2680	70	2451	2217–2719	6 ± 50	marine13
		Carbonate	UCI		75.14	0.81	2300	90	1974	1698–2232	6 ± 50	marine13
		Carbonate	weighted mean				2537	184	2269	1837–2768	6 ± 50	marine13
		Carbonate	corrected mean				2705	223	2479	1918–3024	6 ± 50	marine13
20771	2013-05-22	Graphite	ANSTO	OZT208	63.61	0.19	3635	25	3591	3450–3738	6 ± 50	marine13
		Carbonate	UCI		63.93	0.68	3590	90	3547	3288–3814	6 ± 50	marine13
		Carbonate	corrected				3758	155	3760	3373–4207	6 ± 50	marine13
20772	2013-05-22	Carbonate	UCI		71.93	0.39	2645	45	2392	2188–2604	6 ± 50	marine13
		Carbonate	corrected				2813	134	2603	2235–2925	6 ± 50	marine13
20774	2013-05-22	Carbonate	UCI		77.42	0.41	2055	45	1685	1523–1869	6 ± 50	marine13
		Carbonate	corrected				2223	134	1883	1540–2247	6 ± 50	marine13
21330	2014-06-02	Carbonate	UCI		107.20	0.53			9	5–49		bomb
		Carbonate	corrected		105.11	1.66			10	4–51		bomb

intra-crystalline THAA composition (Fig. 5). The relative concentration of Glu in the intra-crystalline FAA fraction was less than half of its concentration in the THAA. In contrast, the relative concentrations of Asp and Ala in the FAA fraction were higher than in the THAA (Fig. 5). While the concentration of Glu in the intra-crystalline FAA fraction was much lower than in the THAA fraction, the concentrations were still very consistent across analyses as evidenced by the narrow confidence intervals in Fig. 5.

4.3. Within-echinoid-test variation

There was a non-significant difference in the variability of D/L measurements within different test areas (Kruskal Wallis $p = 0.067$), as indicated by the coefficient of variation (CV) calculated from replicate analyses, with oral samples yielding the lowest CV (Fig. 6A). Focusing on the three amino acids with the lowest CV (Fig. 6 and see below), it was apparent the aboral side and lantern CV values were strongly bimodal based on specimen, whereas the oral side and outer edge had more consistent CV values (Fig. 6A). There were significant differences between D/L values measured from the different areas of the test, although there appeared to be little generality to the observed differences (Supplemental Fig. S06). These results indicate it is important to sample a consistent area of the test. The star-shaped pattern of small holes on the aboral side (Fig. 1) may be associated with differences in protein composition or retention in these subsamples. While we

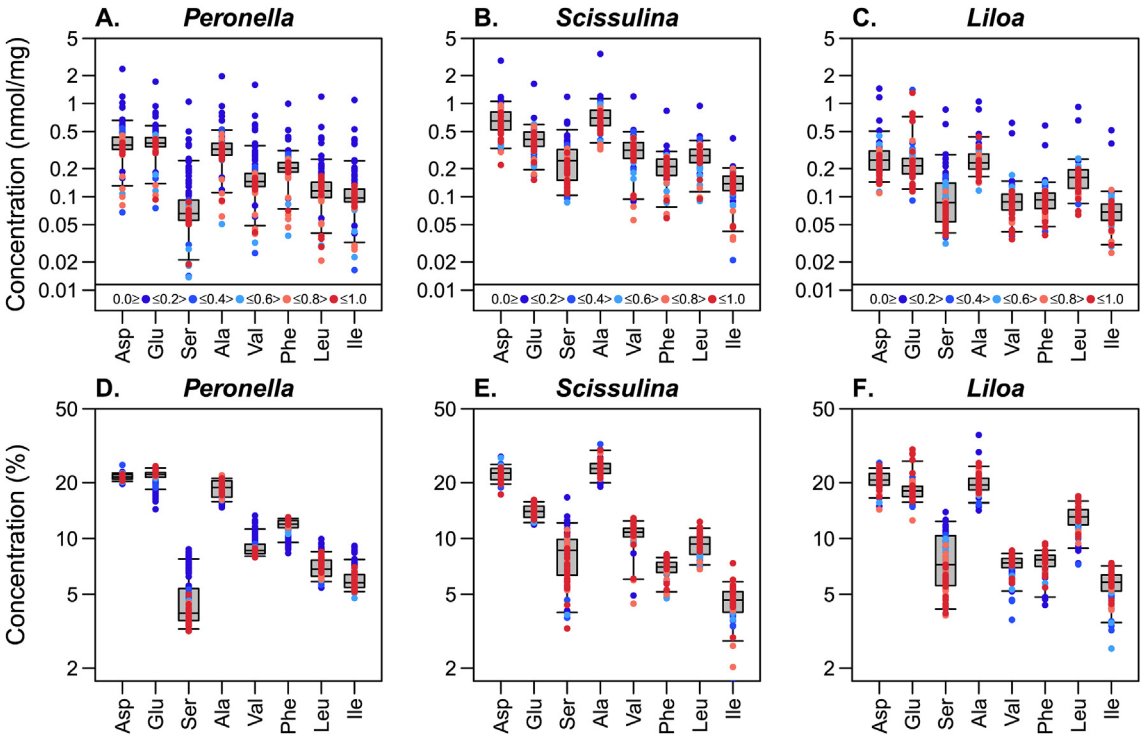

Fig. 4. Comparison of *Peronella* (Echinodermata: Echinoidea), *Scissulina* (Mollusca: Bivalvia) and *Liloa* (Mollusca: Gastropoda) unbleached THAA amino acid composition. Top row (A–C) is amino acid concentration (nmol mg^{-1}), the bottom row (D–F) is the percentage of the total concentration. Both y-axes are log scaled. Points are replicate analyses, colored to indicate the extent of racemization. *Scissulina* and *Liloa* data are from Kosnik et al. (2013).

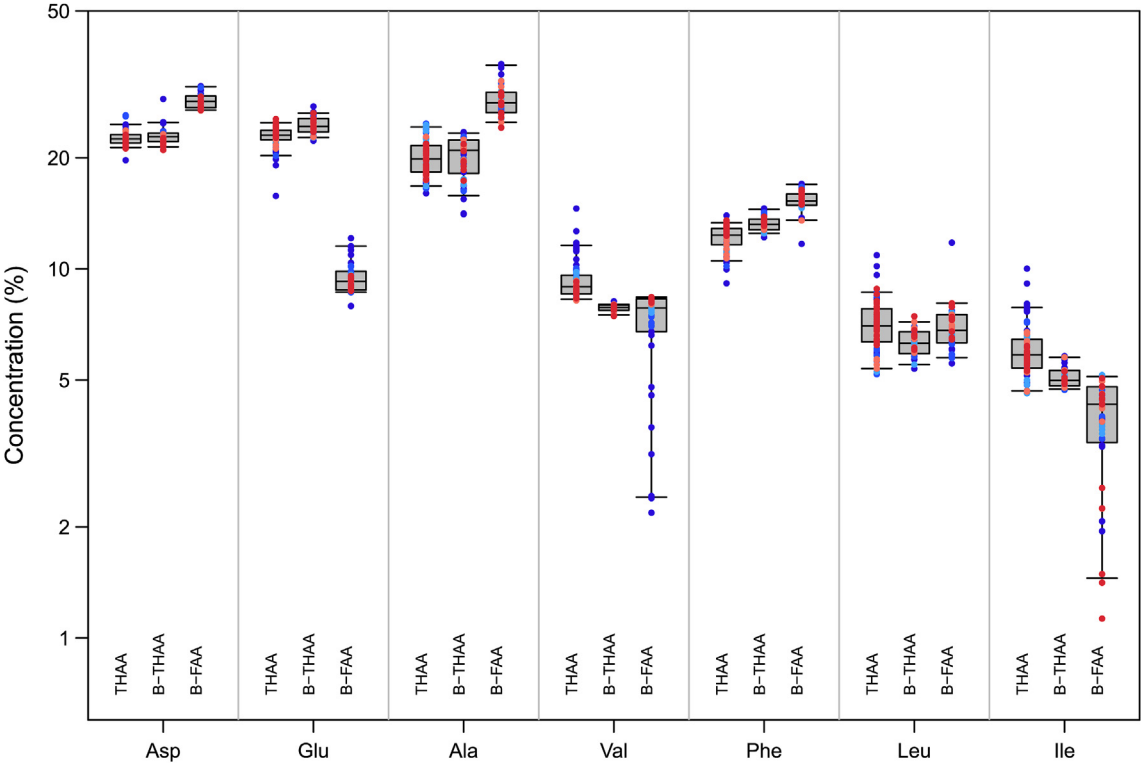

Fig. 5. Relative amino acid composition (percentage) by amino acid fraction for geochronologically useful amino acids in *Peronella*. Points are replicate analyses of unbleached THAA (THAA), bleached (aka, intra-crystalline) THAA (B-THAA), and bleached FAA (B-FAA) fractions from the same 23 specimens colored to indicate the extent of racemization (as in Fig. 4).

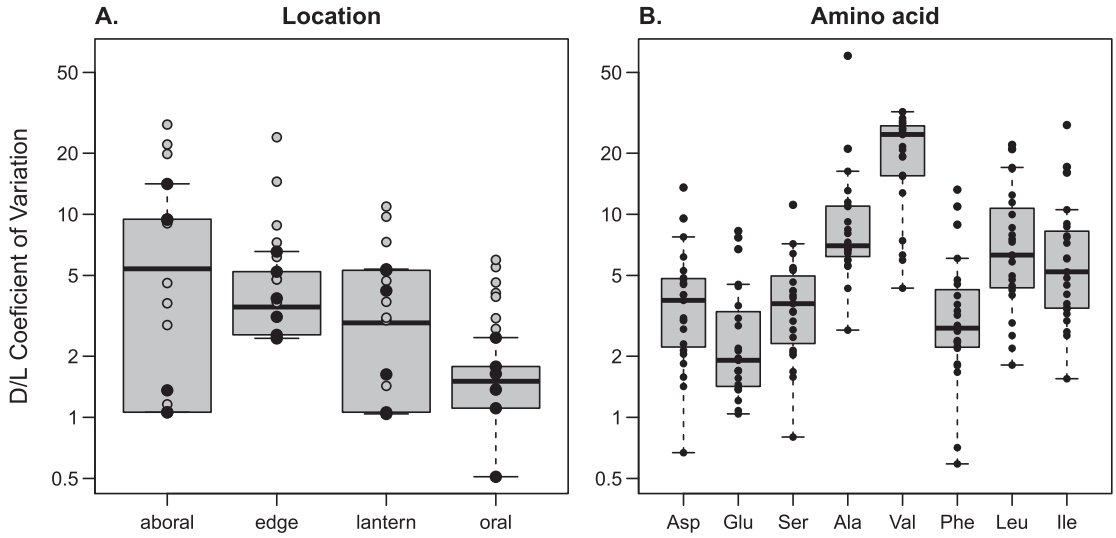

Fig. 6. Box-and-whisker plots of the coefficient of variation (CV) from replicate unbleached THAA D/L measurements of the same tests. Grey boxes indicate interquartile range, the median is indicated by the bold cross bar, the whiskers extend to the most extreme data point no more than 1.5x the interquartile range from the box, and the circles represent CV of D/L values from individual tests. Both panels have identical y-axes showing the CV (log scaled). (A) Replicate samples taken at four locations to determine the variability of different areas of the test. Black circles represent the D/L CV of lower variance amino acids (Asp, Glu and Phe) and grey circles represent higher variance amino acids (Ala, Ile, Leu, Ser, Val). (B) Replicate samples taken from the edge of 23 tests. Four amino acids (Asp, Glu, Ser, and Phe) have lower D/L CV than the other four amino acids (Ala, Ile, Leu, and Val).

did not specifically evaluate this issue, it should be carefully considered if sampling from the aboral side. For the remainder of the analyses presented here, all amino acid data were derived from test fragments taken from the outer edge of the specimens as these are consistently preserved, even in broken specimens.

Twenty-three tests spanning the full range of observed D/L values were used to determine the repeatability of measuring the D/L value of each amino acid in *Peronella* tests. From each specimen three to five subsamples were prepared and analyzed independently. Leu D/L, typically present in low concentrations, was difficult to quantify chromatographically and had the highest CV value (Figs. 2 and 6B). Ala, Val and Ile D/L also had high CV values indicating lower precision measurements (Fig. 6B). Asp, Glu, Ser and Phe all had median CV values < 4% (Fig. 6B). These results indicate Asp, Glu, and Phe were measurable across the observed range of D/L values with a median CV of 2.8% (95th percentile interval: 0.7–12%). This is comparable to previously published molluscan data, with CV values for Asp and Glu of 3.3 and 4.6%, respectively, over a similar range of D/L measurements (Kosnik and Kaufman, 2008).

4.4. D/L covariation

The geochronologically most useful amino acids are those with the lowest CVs (least variability among fragments, as identified above) and with the highest correlation among D/L values. For the unbleached material in our collection, the D/L values for Asp, Glu, and Phe were exceptionally highly related ($r^2 > 0.95$) (Fig. 7). Maximum Glu D/L values were lower than the other two amino acid D/Ls, and had a notably curvilinear relation with Asp and Phe. Asp and Phe D/L had a strong linear relation. The strong covariation in D/L values suggests these amino acid isomers were consistently retained in *Peronella* skeletal mineral, indicating their potential as geochronometers, even in the unbleached material. Within the bleached material (intra-crystalline), the D/L values for these three well-resolved amino acids were also highly correlated between the THAA and the FAA fractions ($r^2 > 0.99$) (Fig. 8). Such congruent geochronological signals suggests closed-system behavior (Collins and Riley, 2000; Preece and Penkman, 2005; Penkman et al., 2007, 2008).

4.5. Amino acids and specimen age

As expected, D/L values derived from all three amino acid fractions examined were strongly related to the radiocarbon age of the specimen (Fig. 9A,C,E). In each of the three low-variance amino acids, bleaching resulted in slightly higher D/L values, although all of the relations were very strong ($r^2 > 0.97$). The r^2 values for relations between D/L and ^{14}C age were both highest and lowest for the bleached FAA, and no fraction performed notably better than any other fraction. The youngest radiocarbon-dated specimen yielded lower-than-expected D/L values in both the intra-crystalline (bleached) B-THAA and unbleached THAA preparations, especially for Phe (Fig. 9E), but these D/L values are consistent with the other very young specimens (Fig. 8).

We also examined the relation between the radiocarbon age of the specimen and amino acid concentration. The concentration of amino acids in the bleached THAA preparation was not related to specimen age ($p > 0.1$), and the concentration of unbleached THAA had only a weak relation to age (Fig. 9B,D,F). The youngest test had a very low concentration of FAA, presumably because the proteins were still largely intact. The relation between specimen age and amino acid concentration (Fig. 9) is heavily influenced by a single young radiocarbon-dated specimen, but the same pattern is also seen in the full dataset. The youngest radiocarbon-dated specimen plots together with other low D/L specimens in Figs. 7 and 8. Together, these patterns indicate amino acids are retained in the sand dollar mineral on timescales of up to ~5 ka, and that amino acid D/L is determined primarily by specimen age.

4.6. Radiocarbon calibration of AAR

Due to age offset between carbonate and graphite targets (see: Section 4.1), we performed the AAR calibration using graphite

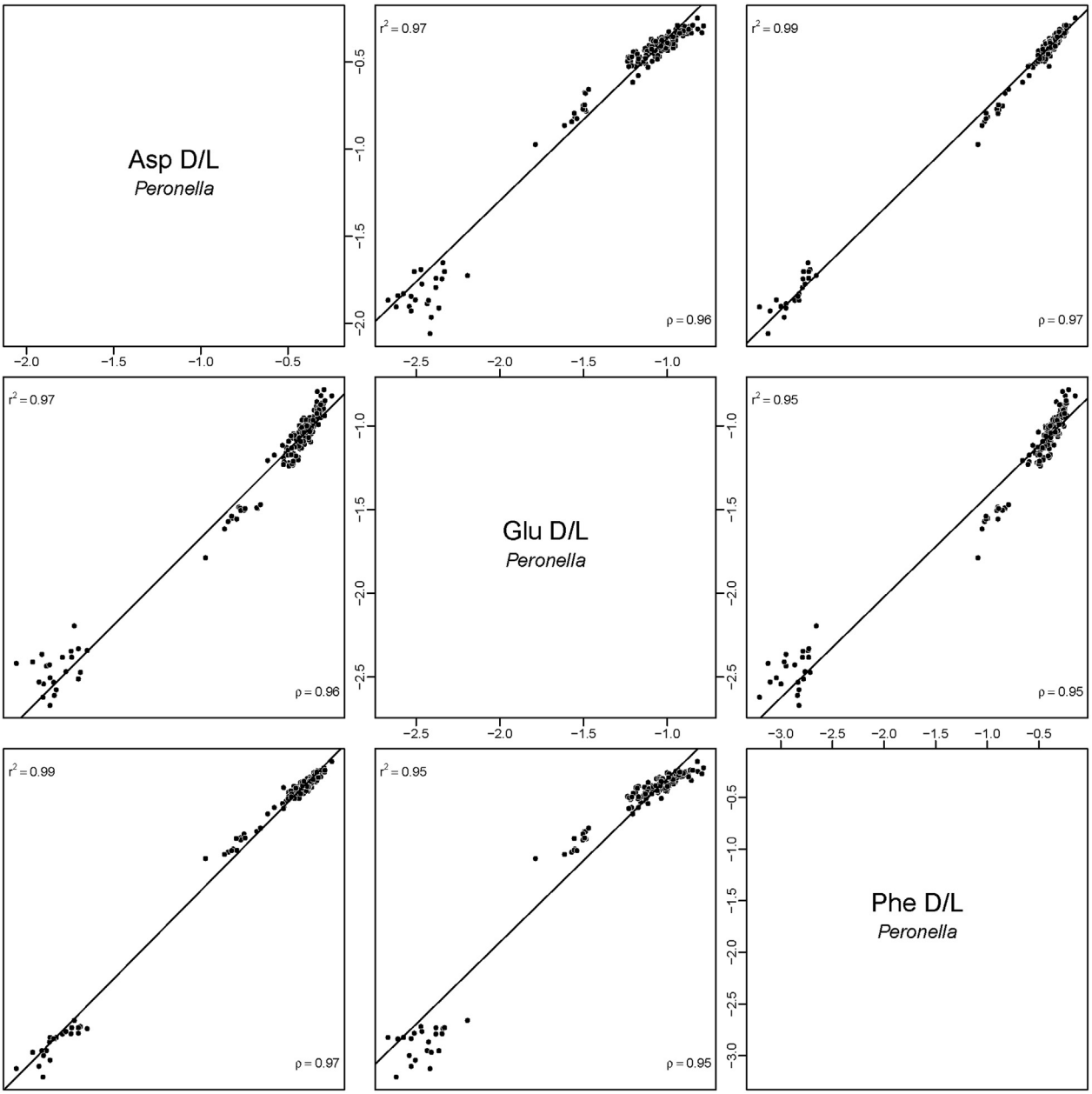

Fig. 7. Correlations between unbleached THAA amino acid D/Ls for the three low-variance amino acids (Asp, Glu and Phe) from replicate samples. The axes are $\log_2$ (D/L) and the same for all axes of each amino acid, but different between amino acids. The solid line represents the best fit relation between $\log_2$(D/L)s. All three $\log_2$(D/L)s are highly correlated, although Asp v. Phe show exceptionally strong linear relations across the range of D/L values, whereas the Glu is slightly non-linear.

target ages for specimens with age estimates from both graphite and carbonate targets. Ultimately the differences between AAR-^{14}C calibrations performed using different sets of radiocarbon ages were minor compared to other sources of variance, and the resulting uncertainty in the AAR-inferred ages was not notably different. This similarity was due, in part, to not explicitly including the uncertainty associated with each radiocarbon age when calculating the AAR-^{14}C calibrations.

Bayesian methods are ideally suited to determining the best amino acids and mathematical functions to model the relation between D/L and age, but evaluating uncertainty distributions and fit versus defined R_0 is inherently more subjective. The model with the lowest Bayesian information criterion (BIC) is typically considered the best model, and models within 4 BIC units of the best model are considered good enough to be included in an averaged model. Ideally the model residuals, which can be heavily influenced by the uncertainty distribution used, have no trend and are uniformly low across the observed age range (Fig. 10 bottom row). In the models evaluated here, trends in the residuals were relatively weak and associated with a particular amino acids rather than particular functions (Appendix B3). There was a notable spread of D/L values for material dated to ~4 ka in all models (Fig. 10, Appendix B3). The importance of these two modeling choices can be examined by plotting the ages inferred using different modeling choices against each other (Fig. 11). Ages inferred using models fit with either uncertainty distribution were

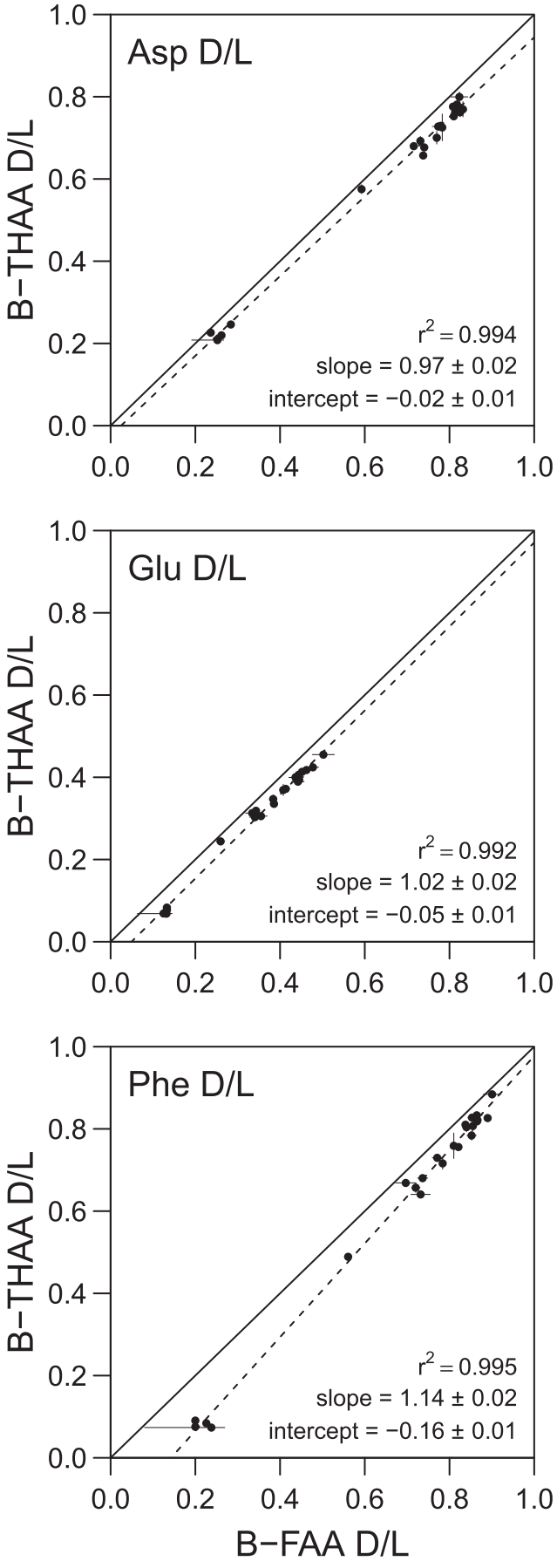

largely unaffected by how R_0 was determined (Fig. 11A and B), whereas ages derived from models with $R_0 \equiv 0$ or fit R_0 were slightly more influenced by which uncertainty distribution was used, as evidenced by fewer points being directly on the unity line (Fig. 11C and D). However, in all cases the inferred uncertainty overlapped the unity line and the impact of these modeling decisions was minor relative to the uncertainty estimates (Fig. 11). Examination of the fit model parameters shows that fit R_0 values ($R_{0\ mean} = 0.027$, Table 2) were slightly higher than typically measured R_0 in live-collected molluscs (see Allen et al., 2013, Table 2). While live-collected material might allow us to better constrain R_0, this was not possible despite considerable effort to find live specimens.

The averaged age model was derived from 36 fit models (3 amino acids [Asp, Glu, Phe], 3 functions [SPK, CPK, TDK], 2 uncertainty distributions [gamma, lognormal], and 2 methods of determining R_0 [$R_0 \equiv 0$, fit R_0]). These 36 models contained three models that were within 4 BIC units of the best fit model, and these three models were averaged using Bayesian model averaging to obtain the final averaged age model (Table 2, Appendix B1). Glu is the only amino acid contributing to the final averaged model (Fig. 10, Table 2). The time-dependent kinetics model made up 45%, and two simple power-law kinetics models made up 55%. Two models fit using lognormal uncertainty made up 90% of the averaged model, and a model fit using gamma uncertainty made up 10% of the averaged model. The small number of informative models was somewhat surprising given the strong covariance observed between amino acids (Fig. 7, $\rho \geq 0.95$, $r^2 \geq 0.95$). The relation between amino acid D/L and radiocarbon age for these low-CV amino acids was also strong (Fig. 9).

Examination of the modeled ages shows that models using either gamma or lognormal uncertainties yielded very similar estimated ages (Appendix B5, median difference between the lognormal gamma model ages was <1%) as well as similar uncertainties (median lognormal model age uncertainty was ±29% and the median gamma model age uncertainty was ±28%). However this obscures two very distinct age populations within the dataset, a set of 16 young individuals dated <300 a, and a set of 57 older individuals >1.5 ka. The uncertainty of the ages of the older specimens was essentially unaffected by the choice of uncertainty distribution (the lognormal model age uncertainty was ±29% versus ± 27% for the gamma model age uncertainty). In contrast, the median uncertainty of the lognormal modeled age estimates for specimens <300 a was ±47% versus ±169% for gamma modeled ages. The relatively broad uncertainties associated with models fit using either uncertainty distribution easily overlap the period when people tried but failed to find living *Peronella* (Miskelly, 2002; Kosnik, pers obs). Ages inferred from models using lognormal uncertainty suggested a population extant in Little Manly Cove between 1963 and 1999 AD, whereas ages inferred from models using gamma uncertainty suggested a population between 1897 and 1960 AD. While these differences are small in the context of the Holocene, they are significant in the context of the rapid development of Sydney during this time period and the desire to precisely determine the timing of faunal changes in the context of changing human impacts (Kosnik and Kowalewski, 2016).

Fig. 8. Relation between bleached (intra-crystalline) FAA D/L (B-FAA D/L) and bleached THAA D/L (B-THAA D/L) for the three low-variance amino acids (Asp, Glu and Phe). The x-axis and y-axis are identical in all panels, the solid line represents 1:1, the dashed line represents the best-fit relation, and the dots represent individual specimens with 95% confidence intervals on those with replicate analyses.

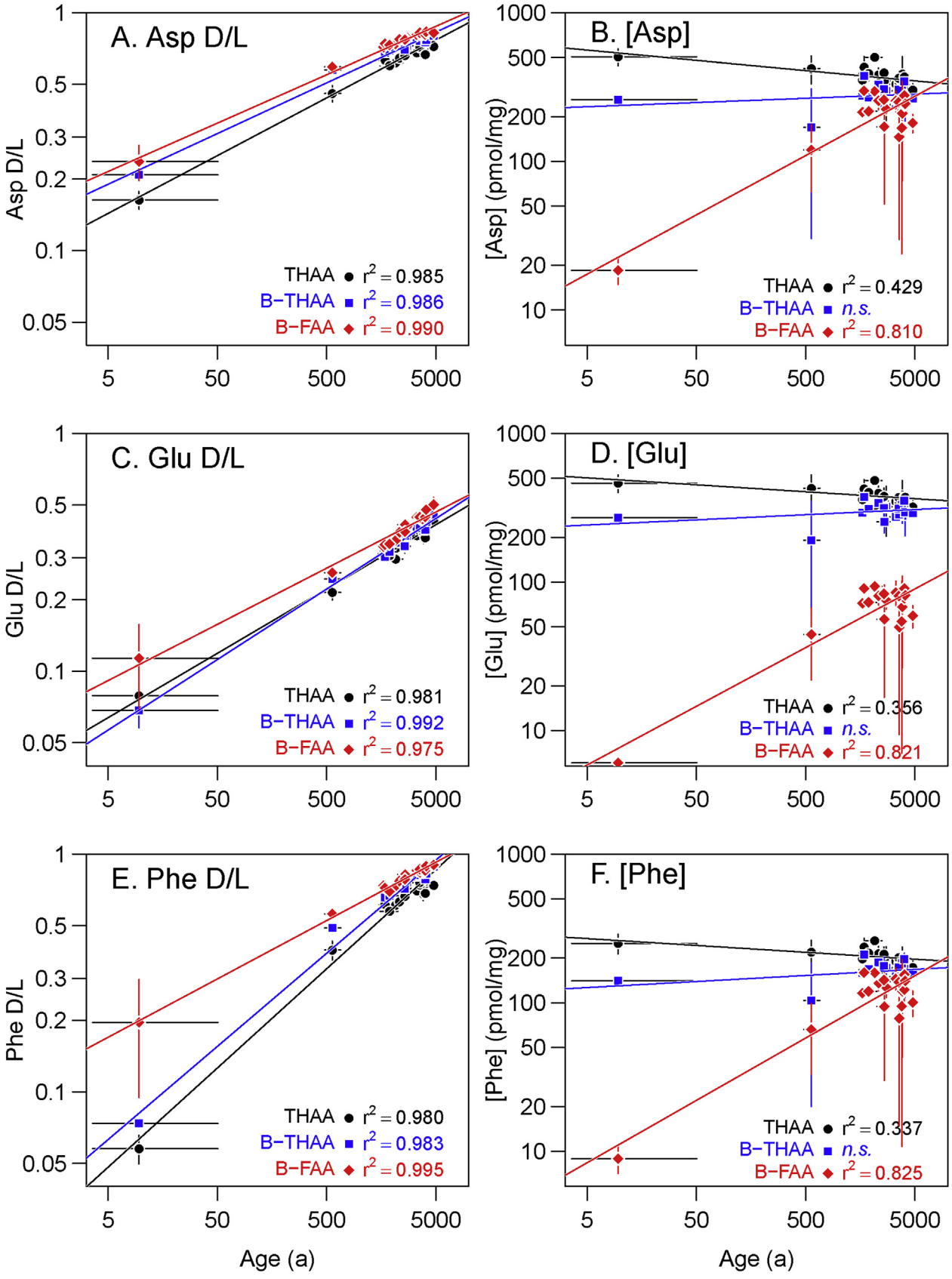

Fig. 9. Relation between the three low-variance amino acid D/Ls, amino acid concentrations and specimen age (years prior to 2013) for unbleached THAA, intra-crystalline THAA (B-THAA) and intra-crystalline FAA (B-FAA) fractions (both x- and y-axes are log scaled). Amino acids in rows, the left column contains amino acid D/Ls and the right column contains total amino acid concentrations. Points are median values of replicate analyses with bars representing 95% confidence intervals. Pearson regression r-squared are listed where the p-value of the regression is less than 0.05.

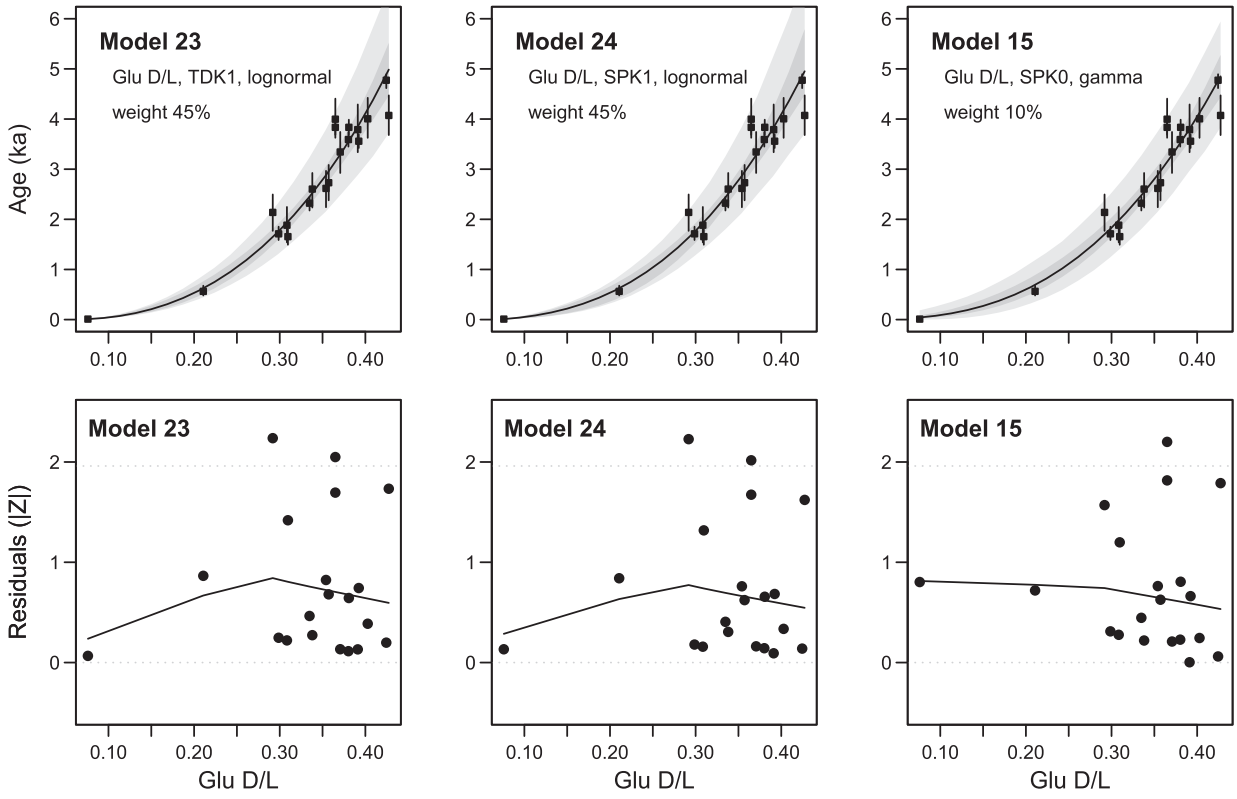

Fig. 10. The three age models contributing to the average age model. Each black circle represents a single dated specimen. The top row shows calibration curves, age (ka) on the y-axes and amino acid D/L on the x-axes. The bottom plots absolute standard residuals (|X|) on the y-axes and amino acid D/L on the x-axes. The amino acid, function, uncertainty distribution and model weight are shown in the top panel for each model, these three models combined make up the Bayesian averaged age model.

While radiocarbon has its own set of potential uncertainties, we doubt they drive the variability observed here. The higher-than-desirable uncertainty in the modeled AAR ages likely arises from two key factors. First is the choice to use subsamples from the edge of tests, despite the higher CV at this location. Second is the notable variation in the AAR- ^{14}C calibration dataset, especially ~4 ka, which is expressed as high residual values (Fig. 10). This D/L variability might only be apparent because a relatively large number of radiocarbon analyses clustered around this age. This points to the need to explore the data in detail rather than simply using the final age model as the only indication of geochronological precision, and it also may suggest that individual echinoid tests racemize at slightly different rates, or it highlights the intra-test variability at the test edge.

5. Conclusions

Holocene echinoderm material appears to be well suited to AAR dating with potentially broad applications to late Quaternary geochronology, taphonomy and paleobiology. Specifically, the results demonstrate the following:

1. *Peronella* tests yield consistently well-resolved HPLC chromatograms, and the amino acid composition is consistent among specimens.
2. Within-test variability is sufficiently high to require that individual tests be sampled consistently from the same anatomical position. For this study, we focused on results from the test edge for the practical reason that they are the most frequently preserved in the stratigraphic record, even though the variability among fragments analyzed from the edge was higher than from other locations.
3. Replicate analyses point to high repeatability, with CV and analytical error for three amino acids (Asp, Glu, Phe) comparable in magnitude to molluscan material and analytical standards.
4. Bleaching to isolate the intra-crystalline amino acid fraction did not substantially improve the relation between D/L and ^{14}C age.

While the uncertainties associated with the ages modeled here are higher than ideal, the ability to date large numbers of relatively recent echinoderm tests opens the possibility of examining a range of interesting palaeobiological and taphonomic questions. Calibrated AAR should enable us to study time-averaging and taphonomy of echinoderm material to complement previous studies hitherto limited to molluscan and brachiopod material. In addition, AAR raises the possibility of directly dating remains from the Caribbean *Diadema* outbreak and collapse (Lessios, 1988) to examine the sedimentary records of this type of event (see Kosnik et al., 2015). AAR geochronology can enable investigations into echinoderm taphonomy and time-averaging similar to those that have recently advanced our understanding of fossilization

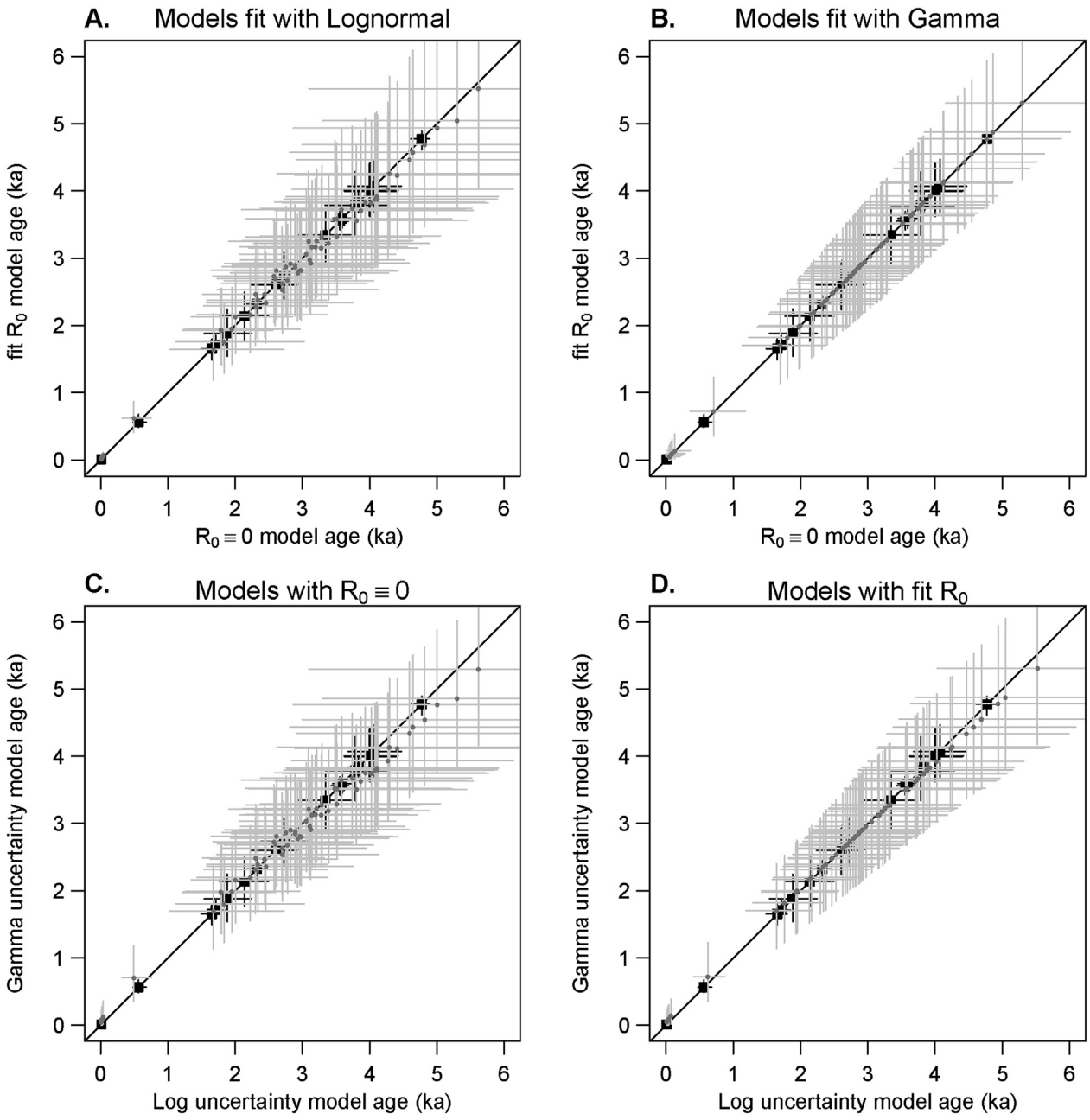

Fig. 11. Comparison of modelled ages (ka) illustrating the relative importance of uncertainty model choice and method of determining R_0. The unity line represents perfect agreement between models. Grey circles and whiskers represent modelled ages with 95% confidence intervals. Black squares and whiskers represent carbon dated specimens (Table 1B). (A) Models assuming lognormal distributed uncertainties were relatively insensitive to R_0 assumption. (B) Models assuming gamma distributed uncertainties were not influenced by the choice of R_0 assumption. (C) Models $R_0 \equiv 0$ showed some variability depending on uncertainty distribution, but the estimated ages are all close to the unity line. (D) Models fit R_0 showed little variability depending on uncertainty distribution, and all of the estimated ages are close to the unity line.

Table 2
The seven AAR age models within six Bayes information criterion (BIC) units of the best model. Where parameters are not fit, they are indicated with NA. "D/L" is the amino acid D/L value, "Distribution" refers to the uncertainty distribution used to fit the model, and "Function" is the mathematical function used to fit the data. The columns ln(a), ln(b), R_0, ln(d) are the maximum likelihood estimates from the model. "ΔBIC" is the difference between the model's BIC and the lowest BIC, "wBIC" is the weight of the model in the final averaged model, "Model" refers to the model numbers used in Appendices B1–B4.

D/L	Distribution	Function	ln(a)	ln(b)	c	ln(R_0)	ln(d)	DIC	n	k	BIC	ΔBIC	wBIC	Model
Glu	lognormal	TDK1	10.57	0.83	0.39	−3.25	−4.29	286.8	20	4	288.79	0.00	0.45	23
Glu	lognormal	SPK1	10.96	1.06	1.24	−2.94	−4.23	294.1	20	4	288.80	0.01	0.45	24
Glu	gamma	SPK0	10.83	1.01	NA	NA	3.75	289.5	20	3	291.75	2.96	0.10	15
Glu	gamma	TDK0	10.50	0.94	NA	NA	3.80	290.6	20	3	293.01	4.22		14
Glu	gamma	SPK1	10.75	0.98	0.91	−3.02	3.63	289.5	20	4	294.20	5.41		18
Glu	gamma	TDK1	10.39	0.78	0.07	−3.46	3.67	290.8	20	4	294.39	5.60		17
Glu	lognormal	CPK1	5.73	1.16	1.76	−2.86	−4.02	292.0	20	4	294.55	5.76		22

processes for molluscs.

Acknowledgements

We thank: members of Australian Navy Clearance Dive Team One, G. Dominguez, and E. Truszewski for assistance collecting the samples; J. Southon for the UCI ^{14}C analyses and discussion of the observed offset between carbonate and graphite target ages; R. Jacob of the Office of Environment and Heritage NSW for the tidal measurements used for site water depth corrections; and K. Wilson for comments on the manuscript. We are grateful for the very thoughtful and constructive reviews provided by J.E. Ortiz and K. Penkman. This work was funded by: U.S. National Science Foundation grant EAR-1234413 (AAR analyses); and Australian Research Council grant FT0990983 (MAK support).

Appendix A. Supplementary data

Supplementary data related to this article can be found at http://dx.doi.org/10.1016/j.quageo.2016.12.001.

References

Agassiz, L., 1841. Monographie d'Echinodermes vivants et fossiles. II. Echinites. Famille des Clypéastroides. Des Scutelles, pp. 1–151 pls 1–27.

Allen, A.P., Kosnik, M.A., Kaufman, D.S., 2013. Characterizing the dynamics of amino acid racemization using time-dependent reaction kinetics: a Bayesian approach to fitting age-calibration models. Quat. Geochronol. 18, 63–77. http://dx.doi.org/10.1016/j.quageo.2013.06.003.

Allison, P.A., 1990. Variation in rates of decay and disarticulation of echinodermata: implications for the application of actualistic data. PALAIOS 5, 432–440. http://dx.doi.org/10.2307/3514836.

Barbour Wood, S.L., Krause, R.A., Kowalewski, M., Wehmiller, J.F., Simões, M.G., 2006. Aspartic acid racemization dating of Holocene brachiopods and bivalves from the southern Brazilian Shelf, South Atlantic. Quat. Res. 66, 323–331. http://dx.doi.org/10.1016/j.yqres.2006.04.001.

Bevington, P.R., Robinson, D.K., 1992. Data Reduction and Error Analysis for the Physical Sciences, second ed. McGraw-Hill Inc., New York.

Bronk Ramsey, C., 2009. Bayesian analysis of radiocarbon dates. Radiocarbon 51 (1), 337–360.

Bush, S.L., Santos, G.M., Xu, X., Southon, J.R., Thiagarajan, N., Hines, S.K., Adkins, J.F., 2013. Simple, rapid, cost effective: a screening method for ^{14}C analysis of small carbonate samples. Radiocarbon 55 (2–3), 631–640. http://dx.doi.org/10.2458/azu_js_rc.55.16192.

Carroll, M., Kowalewski, M., Simões, M.G., Goodfriend, G.A., 2003. Quantitative estimates of time averaging in terebratulid brachiopod shell accumulations from a modern tropical shelf. Paleobiology 29, 381–402. http://dx.doi.org/10.1666/08072.1.

Collins, M.J., Riley, M., 2000. Amino acid racemization in biominerals, the impact of protein degradation and loss. In: Goodfriend, G.A., Collins, M.J., Fogel, M.L., Macko, S.A., Wehmiller, J.F. (Eds.), Perspectives in Amino Acid and Protein Geochemistry. Oxford University Press, New York, pp. 120–141.

Dawson, J.L., Smithers, S.G., Hua, Q., 2014. The importance of large benthic foraminifera to reef island sediment budget and dynamics at Raine Island, northern Great Barrier Reef. Geomorphology 222, 68–81. http://dx.doi.org/10.1016/j.geomorph.2014.03.023.

Demarchi, B., Collins, M.J., Tomiak, P.J., Davies, B.J., Penkman, K.E.H., 2013. Intracrystalline protein diagenesis (IcPD) in *Patella vulgata*. Part II: breakdown and temperature sensitivity. Quat. Geochronol. 16, 158–172. http://dx.doi.org/10.1016/j.quageo.2012.08.001.

Dexter, T.A., Kaufman, D.S., Krause Jr., R.A., Barbour Wood, S.L., Simões, M.G., Huntley, J.W., Yanes, Y., Romanek, C.S., Kowalewski, M., 2014. A continuous multi-millennial record of surficial bivalve mollusk shells from the São Paulo Bight, Brazilian shelf. Quat. Res. 81, 274–283. http://dx.doi.org/10.1016/j.yqres.2013.12.007.

Dominguez, J.D.S., Kosnik, M.A., Hua, Q., Jacob, D.E., Kaufman, D.S., Whitacre, K., 2016. Time-averaging in death assemblages and Holocene deposits: Sydney Harbour's molluscan record. PALAIOS 31, 536–574. http://dx.doi.org/10.2110/palo.2015.087.

Druffel, E.R.M., Griffin, S., 1995. Regional variability of surface ocean radiocarbon from southern Great Barrier Reef corals. Radiocarbon 37, 517–524.

Druffel, E.R.M., Griffin, S., 1999. Variability of surface ocean radiocarbon and stable isotopes in the southwestern Pacific. J. Geophys. Res. 104, 23607–23613.

Fink, D., Hotchkis, M., Hua, Q., Jacobsen, G., Smith, A.M., Zoppi, U., Child, D., Mifsud, C., van der Gaast, H., Williams, A., Williams, M., 2004. The ANTARES AMS facility at ANSTO. Nucl. Instrum. Methods Phys. Res. B 223–224, 109–115.

Greenstein, B.J., 1991. An integrated study of echinoid taphonomy: predictions for the fossil record of four echinoid families. PALAIOS 6, 519–540. http://dx.doi.org/10.2110/palo.2009.p09-144r.

Greenstein, B.J., 1992. Taphonomic bias and the evolutionary history of the family Cidaridae (Echinodermata: Echinoidea). Paleobiology 18, 50–179. http://dx.doi.org/10.1666/0094-8373(2000)26[103:TAP]2.0.CO;2.

Greenstein, B.J., 1993. Is the fossil record of regular Echinoids really so poor? A comparison of living and subfossil assemblages. Palaios 8, 587–601. http://dx.doi.org/10.2307/3515034.

Hua, Q., 2015. Radiocarbon dating of marine carbonates. In: Rink, W.J., Thompson, J. (Eds.), Encyclopedia of Scientific Dating Methods. Earth Sciences Series. Springer, Netherlands, pp. 676–679.

Kaufman, D.S., Manley, W.F., 1998. A new procedure for determining DL amino acid ratios in fossils using reverse phase liquid chromatography. Quat. Sci. Rev. 17, 987–1000. http://dx.doi.org/10.1016/j.quaint.2010.05.029.

Kidwell, S.M., Best, M.M.R., Kaufman, D.S., 2005. Taphonomic tradeoffs in tropical marine death assemblages: differential time-averaging, shell loss, and probable bias in siliciclastic versus carbonate facies. Geology 33, 729–732. http://dx.doi.org/10.1130/G21607.1.

Killian, C.E., Metzler, R.A., Gong, Y.U.T., Olson, I.C., Aizenberg, J., Politi, Y., Wilt, F.H., Scholl, A., Young, A., Doran, A., Kunz, M., Tamura, N., Coppersmith, S.N., Gilbert, P.U.P.A., 2009. Mechanisms of calcite Co-Orientation in sea Urchin tooth. J. Am. Chem. Soc. 131, 18404–18409. http://dx.doi.org/10.1021/ja907063z.

Kosnik, M.A., Hua, Q., Jacobsen, G.E., Kaufman, D.S., Wüst, R.A., 2007. Sediment mixing and stratigraphic disorder revealed by the age-structure of Tellina shells in Great Barrier Reef sediment. Geology 35, 811–814. http://dx.doi.org/10.1130/G23722A.1.

Kosnik, M.A., Kaufman, D.S., 2008. Identifying outliers and assessing the accuracy of amino acid racemization measurements for geochronology: II. Data screening. Quat. Geochronol. 3 (4), 328–341. http://dx.doi.org/10.1016/j.quageo.2008.04.001.

Kosnik, M.A., Kaufman, D.S., Hua, Q., 2008. Identifying outliers and assessing the accuracy of amino acid racemization measurements for use in geochronology: I. Age calibration curves. Quat. Geochronol. 3 (4), 308–327. http://dx.doi.org/10.1016/j.quageo.2008.04.002.

Kosnik, M.A., Hua, Q., Kaufman, D.S., Zawadzki, A., 2015. Sediment accumulation, stratigraphic order, and the extent of time-averaging in lagoonal sediments: a comparison of ^{210}Pb and ^{14}C/amino acid racemization chronologies. Coral Reefs 23, 215–229. http://dx.doi.org/10.1007/s00338-014-1234-2.

Kosnik, M.A., Hua, Q., Kaufman, D.S., Wüst, R.A., 2009. Taphonomic bias and time-averaging in tropical molluscan death assemblages: differential shell half-lives in Great Barrier Reef sediment. Paleobiology 34 (4), 565–586. http://dx.doi.org/10.1666/0094-8373-35.4.565.

Kosnik, M.A., Kowalewski, M., 2016. Understanding modern extinctions in marine ecosystems: the role of palaeoecological data. Biol. Lett. 12 http://dx.doi.org/10.1098/rsbl.2015.0951.

Kosnik, M.A., Kaufman, D.S., Hua, Q., 2013. Radiocarbon-calibrated multiple amino acid geochronology of Holocene molluscs from bramble and Rib Reefs (Great barrier Reef, Australia). Quat. Geochronol. 16, 73–86. http://dx.doi.org/10.1016/j.quageo.2012.04.024.

Kowalewski, M., Serrano, G.E.A., Flessa, K.W., Goodfriend, G.A., 2000. Dead delta's former productivity: two trillion shells at the mouth of the Colorado River. Geology 28, 1059–1062. http://dx.doi.org/10.1130/0091-7613(2000)28<1059:DDFPTT>2.0.CO;2.

Krause, R.A., Barbour, S.L., Kowalewski, M., Kaufman, D.S., Romanek, C.S., Simões, M.G., Wehmiller, J.F., 2010. Quantitative comparisons and models of time-averaging in bivalve and brachiopod shell accumulations. Paleobiology 36 (3), 428–452. http://dx.doi.org/10.1666/08072.1.

Kroh, A., Smith, A.B., 2010. The phylogeny and classification of post-Palaeozoic echinoids. J. Syst. Palaeontol. 8, 147–212. http://dx.doi.org/10.1080/14772011003603556.

Lessios, H.A., 1988. Mass mortality of *Diadema antillarum* in the Caribbean: what have we learned? Annu. Rev. Ecol. Syst. 371–393. http://dx.doi.org/10.1146/annurev.es.19.110188.002103.

Ma, Y., Aichmayer, A., Paris, O., Fratzi, P., Meibom, A., Metzier, R.A., Politi, Y., Addidi, L., Gilbert, P.U.P.A., Weiner, S., 2009. The grinding top of the sea urchin tooth exhibits exquisite control over calcite crystal orientation and Mg distribution. Proc. Natl. Acad. Sci. U. S. A. 106, 6048–6053. http://dx.doi.org/10.1073/pnas.0810300106.

Miller, G.H., Brigham-Grette, J., 1989. Amino acid geochronology: resolution and precision in carbonate fossils. Quat. Int. 1, 111–128.

Miller, G.H., Kaufman, D.S., Clarke, S.J., 2013. Amino acid dating. In: Elias, S.A., Mock, C.J. (Eds.), Encyclopedia of Quaternary Science, second ed. Elsevier, Amsterdam, pp. 37–48.

Miskelly, A., 2002. Sea Urchins of Australia and the Indo-Pacific. Capricornica Publications, Sydney.

Nebelsick, J., 1999. Taphonomic comparison between Recent and fossil sand dollars. Palaeogeography, Palaeoclimatology. Palaeoecology 149, 349–358. http://dx.doi.org/10.1016/S0031-0182(98)00211-9.

Nebelsick, J.H., Kroh, A., 2002. The stormy path from life to death assemblages: the formation and preservation of mass accumulations of fossil sand dollars. PALAIOS 17, 378–393. http://dx.doi.org/10.1669/0883-1351(2002)017<0378:TSPFLT>2.0.CO;2.

Nelbelsick, J.H., 2004. Taphonomy of Echinoderms: introduction and outlook. In: Heinzeller, Nebelsick (Eds.), Echinoderms: München. Taylor and Francis, London, pp. 471–477.

Olszewski, T.D., Kaufman, D.S., 2015. Tracing burial history and sediment recycling

in a shallow estuarine setting (Copano Bay, Texas) using postmortem ages of the bivalve *Mulinia lateralis*. PALAIOS 30, 224–237. http://dx.doi.org/10.2110/palo.2014.063.

Ortiz, J.E., Gutiérrez-Zugasti, I., Torres, T., Gonzáles-Morales, M., Sánchez-Palencia, Y., 2015. Protein diagenesis in *Patella* shells: implications for amino acid racemization dating. Quat. Geochronol. 27, 105–118. http://dx.doi.org/10.1016/j.quageo.2015.02.008.

Penkman, K.E.H., Preece, R.C., Keen, D.H., Maddy, D., Schreve, D.S., Collins, M.J., 2007. Testing the aminostratigraphy of fluvial archives: the evidence from intra-crystalline proteins within freshwater shells. Quat. Sci. Rev. 26, 2958–2969.

Penkman, K.E.H., Kaufman, D.S., Maddy, D., Collins, M.J., 2008. Closed-system behaviour of the intra-crystalline fraction of amino acids in mollusc shells. Quat. Geochronol. 3, 2–25. http://dx.doi.org/10.1016/j.quageo.2007.07.001.

Petchey, F., 2009. Dating marine shell in Oceania: issues and prospects. In: Fairbairn, A., O'Connor, S., Marwick, B. (Eds.), Terra Australis 28: New Directions in Archaeological Science. ANU E Press, Canberra, pp. 157–172.

Plummer, M., 2003. JAGS: a program for analysis of Bayesian graphical models using gibbs sampling. In: Proceedings of the 3rd International Workshop on Distributed Statistical Computing, Vienna, Austria.

Preece, R.C., Penkman, K.E.H., 2005. New faunal analyses and amino acid dating of the lower palaeolithic site at East farm, Barnham, Suffolk. Proc. Geol. Assoc. 116 (3), 363–377. http://dx.doi.org/10.1016/S0016-7878(05)80053-7.

R Development Core Team, 2016. R: a Language and Environment for Statistical Computing. R Foundation for Statistical Computing, Vienna, Austria. http://www.R-project.org.

Reimer, P.J., Bard, E., Bayliss, A., Beck, J.W., Blackwell, P.G., Bronk Ramsey, C., Buck, C.E., Cheng, H., Edwards, R.L., Friedrich, M., Grootes, P.M., Guilderson, T.P., Haflidason, H., Hajdas, I., Hatté, C., Heaton, T.J., Hoffmann, D.L., Hogg, A.G., Hughen, K.A., Kaiser, K.F., Kromer, B., Manning, S.W., Niu, M., Reimer, R.W., Richards, D.A., Scott, M.E., Southon, J.R., Staff, R.A., Turney, C.S.M., van der Plicht, J., 2013. IntCal13 and Marine13 radiocarbon age calibration curves 0-50,000 years cal BP. Radiocarbon 55 (4), 1869–1887. http://dx.doi.org/10.2458/azu_js_rc.55.16947.

Seilacher, A., 1979. Constructional morphology of sand dollars. Paleobiology 5, 191–221.

Wehmiller, J.F., Miller, G.H., 2000. Aminostratigraphic dating methods in Quaternary geology. In: Noller, J.S., Sowers, J.M., Lettis, W.R. (Eds.), Quaternary Geochronology: Methods and Applications, American Geophysical Union Reference Shelf, vol. 4, pp. 187–222.

Yanes, Y., Kowalewski, M., Oritz, J.E., Castillo, C., Torres, T., Nuez, J., 2007. Scale and structure of time-averaging (age mixing) in terrestrial gastropod assemblages from Quaternary eolian deposits of the eastern Canary Islands. Palaeogeogr. Palaeoclimatol. Palaeoecol. 251, 283–299. http://dx.doi.org/10.1016/j.palaeo.2007.04.002.

Yang, L., Killian, C.E., Kunz, M., Tamura, N., Gilbert, P.U.P.A., 2011. Biomineral nanoparticles are space-filling. Nanoscale 3 (2), 603–609. http://dx.doi.org/10.1039/C0NR00697A.